Avalanche structure in a running sandpile model

B. A. Carreras and V. E. Lynch
Oak Ridge National Laboratory, Oak Ridge, Tennessee 37831-8070

D. E. Newman
Department of Physics, University of Alaska–Fairbanks, Fairbanks, Alaska 99709

R. Sanchez
Departamento de Fisica, Universidad Carlos III de Madrid, 28911 Leganes, Madrid, Spain
(Received 11 February 2002; published 18 July 2002)

The probability distribution function of the avalanche size in the sandpile model does not verify strict self-similarity under changes of the sandpile size. Here we show the existence of avalanches with different space-time structure, and each type of avalanche has a different scaling with the sandpile size. This is the main cause of the lack of self-similarity of the probability distribution function of the avalanche sizes, although the boundary effects can also play a role.

DOI: 10.1103/PhysRevE.66.011302 PACS number(s): 45.70.−n, 05.65.+b, 05.40.−a, 52.25.Fi

I. INTRODUCTION

Many systems in nature are governed by self-organized criticality (SOC) [1]. In such systems, relaxation and transport processes occur through events (avalanches) of all sizes. Because all systems have a finite size, an important issue is how transport scales with the system size. An example that emphasizes this point is the case of magnetically confined plasmas. In some regimes, plasma transport seems to be governed by SOC [2,3]. Therefore, to determine the size of a power-producing plant based on fusion reactions, we must know the scaling of plasma transport with system size. Important economic consequences are attached to the accuracy of this scaling.

If the system dynamics has exact self-similar properties, the probability distribution function (PDF) of the event size S, for varying system size L, verifies $P(S,L)=L^{\beta}F(S/L^{\alpha})$. This is the simplest form of scaling with system size. However, even the simpler SOC models, such as the sandpile [1] or the forest-fire model [4], do not obey exact self-similarity [5,6]. Multifractal scaling laws have been found to better describe the finite-size scaling of the numerically evaluated PDFs in the sandpile model [5]. In Refs. [6,7], it has been found that the breakdown of the exact self-similarity of the forest fire was caused by the different spatial structure of the fires. The forest-fire model has two qualitatively different fires that superimpose to give the effective exponents measured in numerical calculations.

Here, we consider the sandpile model and explore the possible structures of the avalanches. In this case, we consider the space-time structure of the avalanches. This allows us to classify the avalanches into different types and study the separate scaling of their size with the system size. This leads to an explanation of the breakdown of the exact self-similarity of the sandpile dynamics.

The rest of the paper is organized as follows. In Sec. II, we introduce the sandpile model. In Sec. III, we discuss a classification of the avalanches based on their space-time structure. We introduce a simple model for avalanches in Sec. IV. This model ignores space correlations and as a result cannot reproduce the tail of the probability functions, but some insight is given into their parametric dependences. In Sec. V, we calculate the probability of avalanches with a given size or duration on the basis of the model. The scaling of these PDFs with the sandpile size and the effect of the boundary are discussed in Sec. VI. Finally, in Sec. VII, we present the conclusions of this paper.

II. SANDPILE MODEL

The sandpile model has been suggested as a paradigm for SOC turbulent plasma transport in magnetic confinement devices [2,3]. The sandpile model has the instability gradients represented by the slope of the sandpile, while the turbulent transport is modeled by the local amount of sand that falls (overturns) when the sandpile becomes locally unstable. A random ''rain'' of sand grains drives the sandpile. This drive models the input power/fuel in the confinement system. The sandpile model allows us to study the dynamics of the transport independent of both the local instability mechanism and the local transport mechanism.

The PDF of the transport events is one of the measurable quantities, and the experimentally measured ones can be compared to theoretical expectations. Even in the simple sandpile model, the finite-size scaling of the PDFs is complicated and has a multifractal character [5]. Therefore, it is important to understand the underlying structure of the avalanches that causes the multifractal nature of the scaling.

Here, we use a standard cellular automata algorithm [5,8] to study the dynamics of the driven sandpile and the corresponding avalanche structure. The sandpile is constructed over a one-dimensional (1D) domain. This domain is divided into L cells that are evolved in steps. The number of sand grains in a cell is h_i, called the height of cell i. We take as radial position the value i that identifies the cell. The local gradient is Z_i, the difference between h_i and h_{i+1}, and Z_{crit} is the critical gradient. The sandpile evolution is governed by the following simple set of rules.

(1) We add a grain of sand at a randomly selected position i,

$$h_i = h_i + 1. \tag{1}$$

No more sand is added while an avalanche is in progress.

(2) Next, all the cells are checked for stability against a simple stability rule and either flagged as stable, $Z_i < Z_{\text{crit}}$ or not stable, $Z_i \geqslant Z_{\text{crit}}$.

(3) Finally, the cells are time advanced, with the unstable cells overturning and moving their excess grains to another cell. That is, if $Z_i \geqslant Z_{\text{crit}}$, then

$$h_i = h_i - N_f,$$

$$h_{i+1} = h_{i+1} + N_f, \tag{2}$$

where N_f is the amount of sand that falls in an overturning event.

We have modified rule (1) from previous studies [3], where grains of sand were dropped with a given probability p_0. To study the properties of the avalanches, such as the size and duration, it is useful to go to the limit of completely separated avalanches. That is, the case when $p_0 \to 0$. To reach this limit, we change this rule.

III. SPACE-TIME AVALANCHE STRUCTURE

An avalanche can be characterized by several parameters. One is its length l, which is the number of cells affected by the avalanche. Another is its duration T, the number of time steps taken by the avalanche to run through the system. A third parameter is its size S, which is the total number of overturning events during the avalanche. All of these are measurable quantities that can be used in the determination of the space-time structure of the avalanches. To determine how these parameters relate to the avalanche structure, it is useful first to visualize them. In this way, we identify the structures that we want to characterize.

A way of visualizing the avalanches in a running sandpile is to construct a two-dimensional (2D) grid with the X axis being time and the Y axis being cell position. In this grid, we can mark the position and time of each overturned event. In Fig. 1, we show three examples of these types of plots. In looking at such a plot, we can classify the avalanche structure in three distinct ways.

(1) The 1D avalanches. A 1D avalanche is a simple straight line in the space-time plot. An example is shown in Fig. 1(a). For these avalanches, their length, duration, and size are equal: $l = T = S$. These avalanches can cause internal transport within the pile, or they can also cause transport out of the pile when they reach the edge. Reaching the edge does not change the structure of the avalanche, it only limits its length. The amount of flux transported out is obviously N_f.

(2) The 2D avalanches with no flux out. An example is shown in Fig. 1(b). In the space-time plane, these avalanches have a rectangular shape. To better characterize its shape, it is useful to introduce two new parameters. They are the two sides of the rectangle, n and T_0, as defined in Fig. 1(b). By convention, we denote by n the shortest side, $n \leqslant T_0$. There

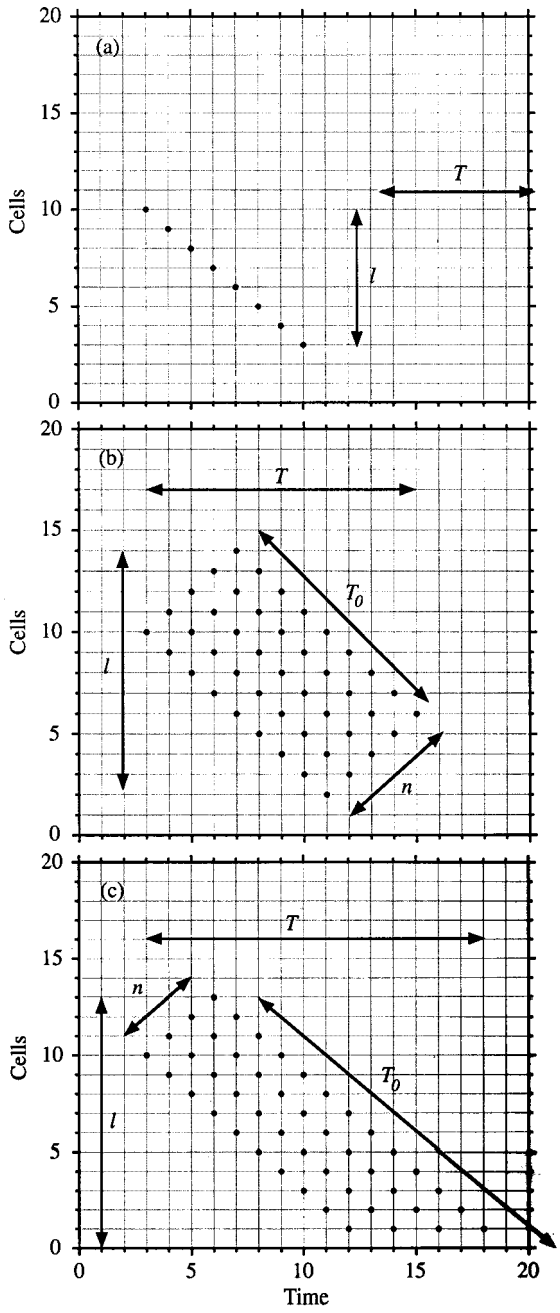

FIG. 1. 2D plot of overturn events (dots) with the X axis being time and the Y axis the cell position: (a) an example of 1D avalanche, (b) an example of 2D avalanche with no flux out, and (c) 2D avalanche with flux out of the sandpile.

is a simple relation between these parameters and the size and the length of the avalanche. For these avalanches, $l = T$.

Then, in terms of the new parameters, the avalanche duration and size are as follows:

$$T = T_0 + n - 1, \tag{3}$$

$$S = nT_0 = n(T - n + 1). \tag{4}$$

From these relations, we can calculate the parameter n as

$$n=\tfrac{1}{2}[T+1-\sqrt{(T+1)^2-4S}]. \quad (5)$$

This is a useful parameter to classify the 2D avalanches. When we measure the size and the duration of an avalanche, Eq. (5) provides a way of testing the structure. To be a 2D avalanche without flux out, n must be an integer. Note that Eq. (5) works also for 1D avalanches, n, there is a maximum and a minimum value of the avalanche size. They are

$$S_{\max}=n(L+1-n),$$

$$S_{\min}=n^2. \quad (6)$$

These values correspond to $T=l=L$ and $n=T_0$, respectively.

(3) The 2D avalanches with flux out of the sandpile. An example of such an avalanche is shown in Fig. 1(c). The space-time structure of these avalanches is somewhat different from the previous one and so are the relations between the main parameters.

In this case, $l=T_0$. The expression for the duration T is the same as Eq. (3), but the avalanche size in terms of n is given by

$$S=n(T+1-n)-\tfrac{1}{2}n(n-1). \quad (7)$$

This leads to the following expression for n in terms of S and T:

$$n=\tfrac{1}{3}[T+\tfrac{3}{2}-\sqrt{(T+\tfrac{3}{2})^2-6S}]. \quad (8)$$

Again, the value of n must be an integer. The flux out of the sandpile is $\Gamma_{\text{out}}=nN_f$. Therefore, using Eqs. (8) and (5), we can determine whether the avalanche has flux out and calculate the value of the flux.

For these avalanches, the maximum and minimum value of their size for a fixed n are

$$S_{\max}=n\left(L+1-\frac{n}{2}\right),$$

$$S_{\min}=\frac{n(n+1)}{2}. \quad (9)$$

In comparing Eqs. (6) and (9), we see that the maximum size of the avalanches that produces a flux out of the pile can be larger than the maximum size of the internal avalanches. It is interesting to compare the boundaries defined by Eqs. (6) and (9) for a given sandpile size. The largest avalanches are those starting near the edge and penetrating all the way to the top of the piles. These avalanches also produce the maximum flux out. These avalanches are the more resilient ones to additional effects such as diffusion [9,10].

In what follows, we will study the scaling of avalanches with no flux out. The ones with flux out occur close to the boundary, and they are a very small fraction of the total number of the avalanches. They only affect the PDFs for very large values of the events. We will consider them in the last section dedicated to boundary effects.

IV. PROBABILITY OF AN AVALANCHE FOR A GIVEN VALUE OF *n*

To better understand the distribution of avalanches with different n values, we consider a very simple statistical model for the avalanches. This model is not going to provide an explanation of the PDF of T and S because it does not incorporate correlation effects that are essential in the generation of the algebraic tails. However, it is a useful model to understand some properties of those probability distributions.

Let p_1 be the probability for a cell to be unstable when N_f grains of sand are added to this cell. This means that an avalanche reaching this cell has a probability p_1 of continuing its propagation. Here, we assume that this probability does not depend on the position of the cell. This implies the neglect of radial correlation, which in reality is important. If a cell is unstable to the addition of N_f grains, this means that the local slope has N_f possible values, $Z_c \geqslant Z \geqslant Z_c-N_f+1$. We know [11] that those N_f states are probably approximately equal. Therefore, the probability of the slope having a given value in this range is p_1/N_f. Conversely, $p_2=1-p_1$ is the probability for a cell to be stable when N_f grains are added. A cell stable to the addition of N_f grains of sand is a stopping position for the avalanche. Let us also assume that p_A is the probability of starting an avalanche, and p_A is practically independent of the cell position. Numerical calculations show a very flat distribution of the starting positions of the avalanches. We will discuss later the form of this probability.

Within the framework of this model, we can now evaluate the probability of an $n=1$ avalanche starting in cell i. To be a $n=1$ avalanche, either the $i+1$ or $i-1$ cells must be a stopping point. Therefore, the probability $P(1)$ of such an avalanche is

$$P(1)=p_A(2p_1p_2+p_2^2)=p_A(1-p_1^2). \quad (10)$$

Although this estimate seems correct, there is one important point that we have not taken into account. An avalanche starts when a grain of sand is dropped on a cell i, such that $Z_i=Z_c$. The addition of a grain at position i changes also the sandpile slope at position $i-1$, which is reduced by 1. This change of slope implies that the cell $i-1$ can only be in one of the N_f-1 states in the range $Z_c \geqslant Z \geqslant Z_c-N_f+1$. Therefore, the probability for the cell $i-1$ to be unstable is really $p_1(1-1/N_f)$, and the probability to be stable is p_2+p_1/N_f. The estimate given by Eq. (10) must be changed to account for this effect. The result is

$$P(1)=p_A[1-p_1^2(1-1/N_f)]. \quad (11)$$

From this expression, we trivially estimate the fraction of $n=1$ avalanches dividing $P(1)$ by p_A. Note that for $N_f=1$, this fraction is 1, as it should be. This expression for the fraction of 1D avalanches agrees very well with the numerical results. In Fig. 2, we plotted, as a function of $1-1/N_f$, the fraction of 1D avalanches obtained in a sequence of numerical calculations for different values of N_f. For these calculations, we have used an $L=1600$ sandpile with Z_c

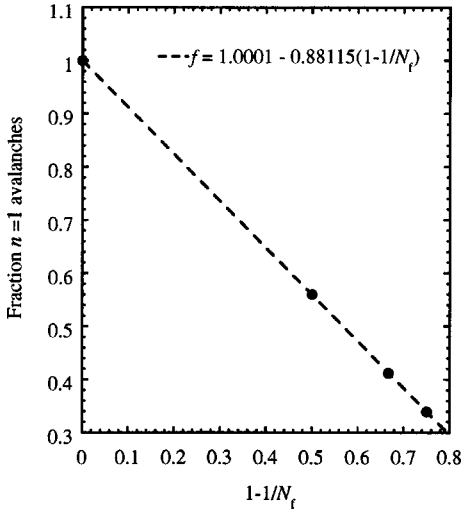

FIG. 2. Fraction of $n=1$ avalanches as a function of $1-1/N_f$.

$=10$. A linear fit to the numerical results gives a value for p_1^2 of about 0.9. We will see later how this value scales with L.

We can now carry out similar calculations for each value of $n>1$ and obtain the probability distribution of avalanches with a given $n>1$ value. In doing so, we obtain

$$P(n)=p_A(1-1/N_f)(1-p_1^2)p_1^{2(n-1)}. \tag{12}$$

Adding n over all, we have

$$\sum_1^{n_{\mathrm{Max}}} P(n)=p_A[1-(1-1/N_f)p_1^{2n_{\mathrm{Max}}}]\approx p_A, \tag{13}$$

as expected.

Using the obtained value of $p_1^2=0.9$, we can compare the fraction of avalanches with a given value of n that we have

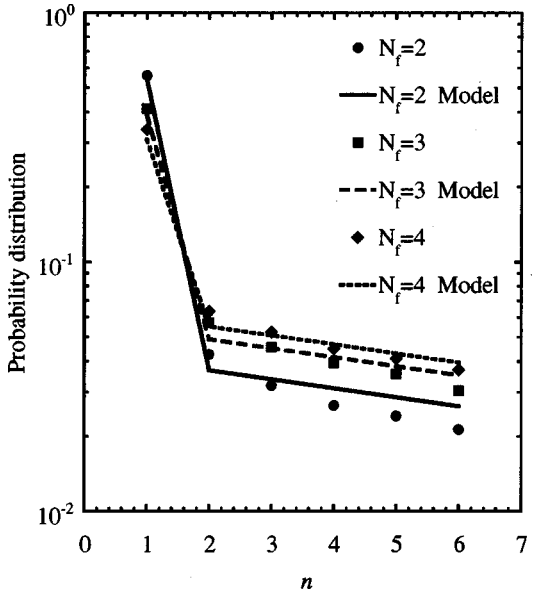

FIG. 3. Comparison of the model with the numerical results for low values of n.

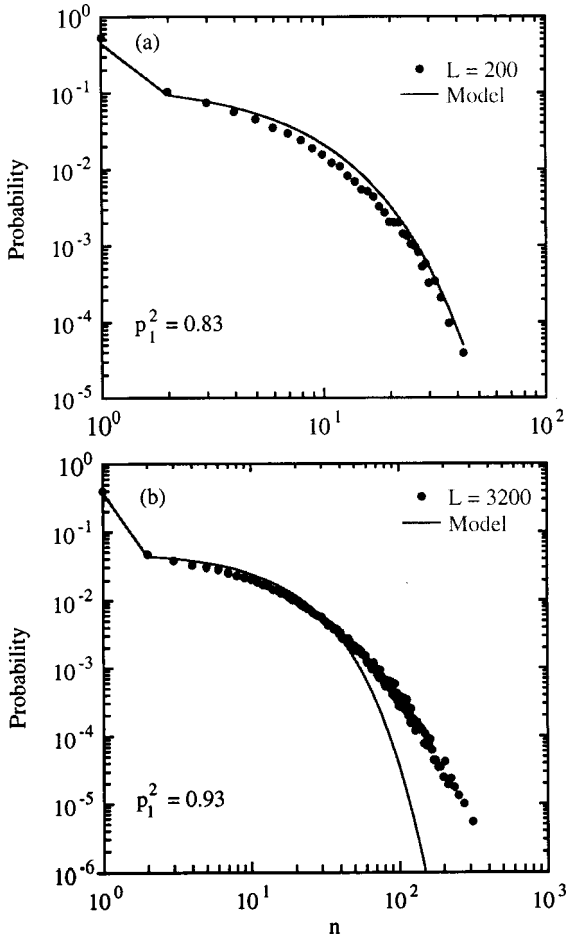

FIG. 4. Comparison of the model with numerical results for two different sandpile lengths: (a) $L=200$ and (b) $L=3200$.

obtained in numerical calculations with the model just discussed. We can see in Fig. 3 that there is good agreement. This model accounts for the significant difference between the 1D avalanches and the 2D ones. This asymmetry is caused by the change of the probabilities in the cell $i+1$ as discussed above.

The agreement between numerical results and the analytical model changes for high-n values. Equation (12) can simply be rewritten in the following way:

$$P(n)=p_A(1-1/N_f)(1-p_1^2)\exp[(n-1)\ln(p_1^2)]. \tag{14}$$

This expression shows that for high n values, the probability decays exponentially with n. Such a high-n tail is surprisingly consistent with the numerical results for a small sandpile, with $L<300$. However, for larger sandpiles, there is a clear discrepancy at high n. An algebraic tail seems to be developing at the high n values. The model discussed here cannot describe such a tail, because it ignores correlations that are the dominant effect in creating large events. A comparison of the model with the numerical data for large n is given in Fig. 4 for two sizes of the sandpile, $L=200$ and $L=3200$.

In comparing the model to the data, we have p_1 as a free parameter. This parameter can be determined by the fraction

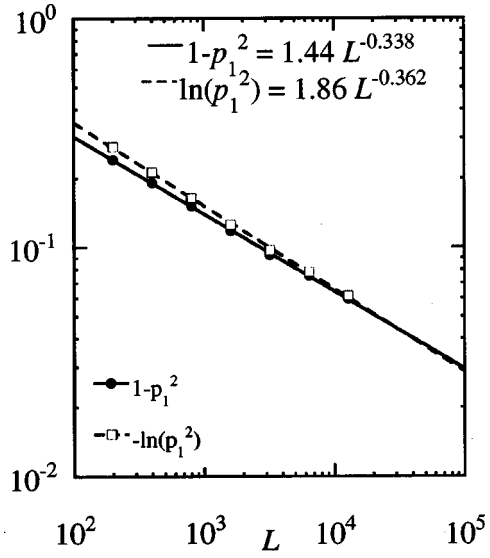

FIG. 5. Scaling of p_1 with the size of the sandpile.

of 1D avalanches, as discussed above, or by a fit to the low-n region of the $P(n)$. The results are not very sensitive to the method of determination of p_1. In whatever way we use to determine p_1, the value of this parameter scales with the size of the sandpile. This scaling is shown in Fig. 5. Because p_1 is always close to 1 and the changes with L are small, we have plotted $1-p_1^2$ and $\ln(p_1^2)$ as a function of L. Both have very similar values because p_1 is close to 1 and they scale as a fractional power of L. Taking $\delta \equiv -\ln(p_1^2) \approx 1-p_1^2$ and for $\delta \ll 1$, we can rewrite Eq. (14) as

$$P(n,\delta) \equiv P(n) \approx p_A(1-1/N_f)\,\delta \exp[-(n-1)\,\delta] = \delta G[(n-1)\,\delta].$$

Because δ has a simple scaling with size, this suggests the existence of a self-similar transformation that accounts for the finite-size effects.

Although we have assumed in the analytical model that there are no radial correlations, in reality there are. We can calculate the correlation of the slope of the sandpile at different radial positions, $\langle Z_i Z_j \rangle$. What we observed is that $\langle Z_i Z_j \rangle \approx \delta_{ij} + c e^{-|x_i - x_j|/\ell}$, with the exponential tail being different for left and right. The coefficient c is always less than 0.3, therefore, the correlations are weak. Nevertheless, the correlations are not negligible. The correlation length scales with the size L, $\ell \approx 0.2 L^{0.8}$, and seems to be independent of N_f. This information on the radial correlation of the slope is not included in the model, but in fitting the numerical results it is reflected in the p_1 dependence on L.

V. PROBABILITY OF AVALANCHES WITH A GIVEN DURATION OR SIZE

Let $P_D(T)$ be the probability of avalanches with duration T. Here we are still considering only avalanches with no flux out. We can decompose this function as a sum over the probabilities of avalanches with duration T and index n,

$$P_D(T) = \sum_{n=1}^{(T+1)/2} P_D(n,T). \tag{15}$$

A similar thing can be done for the probability $P_S(S)$ of avalanches of size S,

$$P_S(S) = \sum_{n=1}^{\sqrt{S}} P_S(n,S). \tag{16}$$

Note that in this sum, for a fixed value of S not all n's can contribute; S must be divisible by the values of n contributing to the sum. For the components $P_D(n,T)$ when summing over all possible values of the avalanche duration for a fixed n, we should recover the probability of an avalanche with this given value of n,

$$P(n) = \sum_{T=2n-1}^{L} P_D(n,T). \tag{17}$$

Similarly when we sum $P_S(n,S)$ over all avalanche sizes for a fixed n, we have

$$P(n) = \sum_{S=n^2}^{n(L+1-n)} P_S(n,S). \tag{18}$$

In spite of the limited value of the model described in Sec. IV, it is worthwhile to use it in evaluations of the different probability functions just defined. We begin by evaluating the probability of avalanches with a fixed value of n and T, or n and S. To do so, it is easier to first calculate the probability of an avalanche with a given n and T_0 value, $P(n,T_0)$. We follow the same approach as before, by evaluating at each step the probability for the avalanche growing or stopping. For an $n=1$ avalanche, the probability of having a length T_0 is

$$P(1,T_0) = p_A[\sigma(1-p_1)(1-1/N_f) + 1/N_f] p_1^{T_0-1} p_2. \tag{19}$$

The p_2 term indicates that after T_0 steps, the avalanche stops at the up or down propagation. We can similarly calculate the corresponding probability for $n \neq 1$ avalanches as

$$P(n,T_0) = \sigma p_A (1-1/N_f) p_1^{n-1} p_1^{T_0-1} p_2^2. \tag{20}$$

The factor σ is 1 for $T_0 = n$ and is equal to 2 for all other values of T_0. For a given n, there is a unique relation between T_0 and T or S. Therefore, we can automatically calculate the probability for an avalanche with given n to have a duration T or a size S. We do that by just substituting T_0 for its expression in terms of T or S into the previous equations. For the $n=1$ avalanches, the changes are trivial because $T_0 = T = S$, then

$$P_D(1,T) = p_A[2(1-p_1)(1-1/N_f) + 1/N_f] p_1^{T-1} p_2,$$

$$P_S(1,S) = p_A[2(1-p_1)(1-1/N_f) + 1/N_f] p_1^{S-1} p_2, \tag{21}$$

when $T=S>1$. For the 2D avalanches with no flux out, we use Eqs. (3) and (4) to relate T_0 to T and S, respectively. When $T>2n$, $S>n^2$, and $n\neq 1$,

$$P_D(n,T)=2p_A(1-1/N_f)p_1^{T-1}p_2^2, \tag{22}$$

$$P_S(n,S)=2p_A(1-1/N_f)p_1^{n+S/n-2}p_2^2. \tag{23}$$

From Eq. (15), we can now calculate the probability of avalanches of duration T,

$$P_D(T)=p_Ap_1^{T-1}(1-p_1)[1/N_f+T(1-1/N_f)(1-p_1)], \tag{24}$$

and the probability of avalanches with size S,

$$P_S(S)=\sigma p_Ap_2\Bigg\{[2(1-p_1)(1-1/N_f)+1/N_f]p_1^{S-1} + 2(1-p_1)(1-1/N_f)\sum_{n=n_{\min}}^{\sqrt{S}}p_1^{n+S/n-2}\Bigg\}. \tag{25}$$

There is not a compact expression that can be derived for Eq. (25) for all values of S. However, it is possible to derive an asymptotic form for $S\gg 1/|\ln p_1|$,

$$P_S(S)\approx\frac{p_Ap_2}{p_1}\Bigg\{\left[2p_2\left(1-\frac{1}{N_f}\right)+\frac{1}{N_f}\right]e^{S\ln p_1} + \frac{p_2}{p_1}\frac{1-1/N_f}{|\ln p_1|}e^{\sqrt{S}\ln p_1}\Bigg\}. \tag{26}$$

The first term in Eq. (26), the contribution from 1D avalanches, depends on $S|\ln p_1|$, while the second term, contribution of the 2D avalanches, depends on $\sqrt{S}|\ln p_1|$. We can see that it is not possible to use a single combination of the variables S and $\ln p_1$ that gives the dependence of the overall function. Therefore, the probability of the avalanches with size S is not a self-similar function. The different dependences of the 1D and 2D avalanches is the cause of the breakdown of self-similarity. Because Eq. (26) is only an asymptotic form for the function $P_S(S)$, it is not clear that the separate functions for the 1D and 2D avalanches are exactly self-similar. There it may be nonasymptotic terms that cause a weak breaking of the individual self-similarity.

The probabilities $P_D(T)$ and $P_S(S)$ have an exponential tail for large S and T. This dependence does not agree with the numerical calculations, but some of the properties of these functions may have a more general relevance.

There is another interesting property of these probabilities. The probability for an avalanche with a given value of $n\neq 1$ to have a duration T is independent of the value of n. That is, for $n\neq 1$,

$$P_D(n,T)=F(T). \tag{27}$$

This property has allowed us to find a compact expression, Eq. (24), for the probability of avalanches with duration T. Another consequence of this relation is

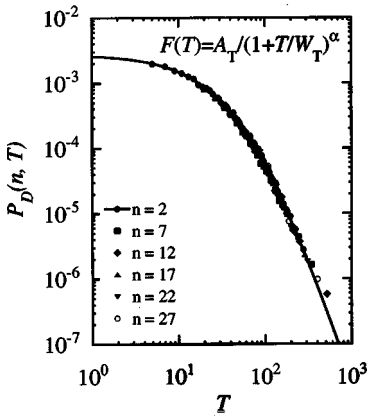

FIG. 6. Function describing $P_D(n,T)$ for different values of n.

$$P_S(n,S)=F\left(\frac{n^2+S}{n}\right). \tag{28}$$

If these relations are true, in general, they imply that the knowledge of the function F gives all the information needed on the probabilities of the 2D avalanches. This does not extend to the 1D avalanches, which have a different functional dependence. Note that the generic normalization conditions from Eq. (17) suggest that such a relation should be true.

We can directly test Eq. (27) using numerical results. In Fig. 6, we have plotted $P_D(n,T)$ for different values of n. The calculation is for an $L=3200$ sandpile with $N_f=3$. We can see that all curves fall on top of each other defining the function $F(T)$. This function is well described through a simple function as shown in the figure with a power tail exponent $\alpha=4\pm 1.5$. Having identified this function F, we can evaluate the distribution $P(n)$ of avalanches for different n. From Eq. (17),

$$P(n)=\sum_{T=2n-1}^{L}F(T). \tag{29}$$

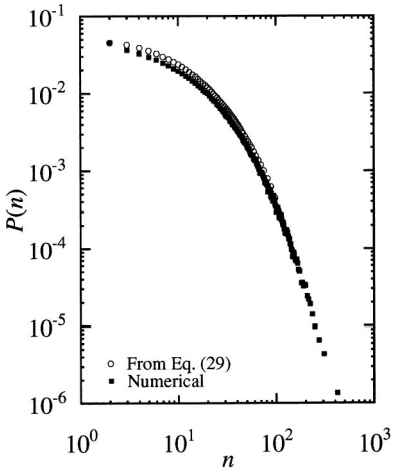

FIG. 7. Comparison of Eq. (29) with $P(n)$ from the numerical results.

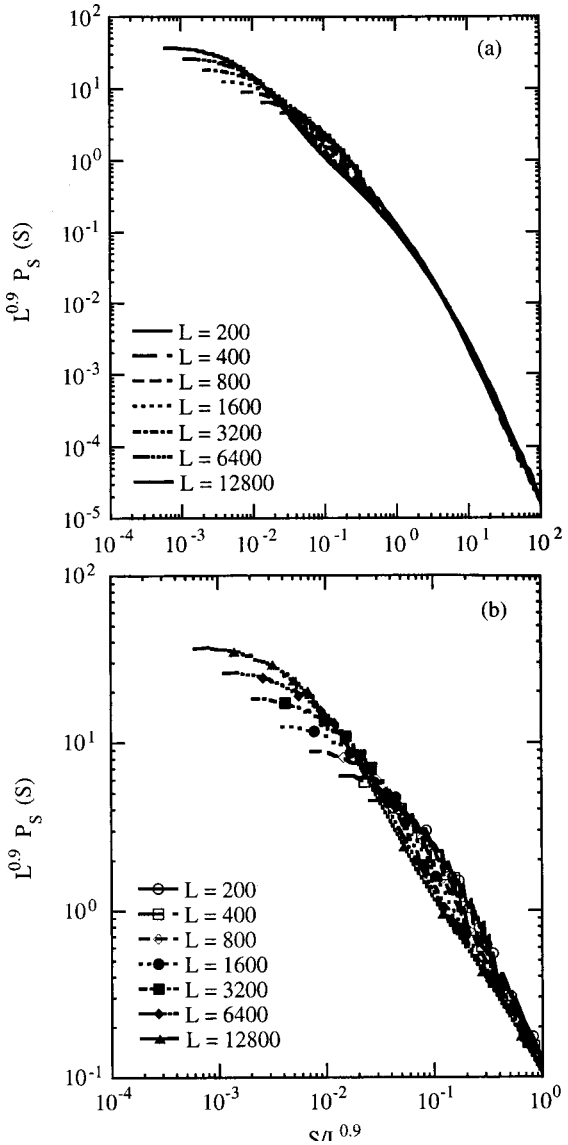

FIG. 8. PDF of the avalanche size for different lengths of the sandpile: (a) the full PDF and (b) PDF for small values of S/L^{α} showing the lack of self-similarity.

In Fig. 7, we compare the $P(n)$ calculated from Eq. (29) with the directly evaluated $P(n)$ from the numerical calculation.

VI. FINITE-SIZE SCALING

We have examined the probability of avalanches of a given duration or size. Now we turn to the dependence of these probabilities on the size of the sandpile. Because we use a numerical scheme for $p_0 \to 0$ in order to avoid avalanche overlap, we cannot calculate the probability of an avalanche of a given size or duration. Instead of the probability, we evaluate the PDF of the avalanche size and duration. The PDFs are equivalent to the probabilities, but they are normalized to 1 instead of being normalized to the frequency of the avalanches.

From Ref. [5], we know that the dependence of the PDF

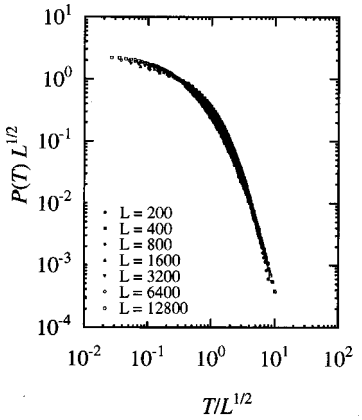

FIG. 9. PDF of the size of the 1D avalanches.

of the avalanche size on L is not a simple self-similarity relation, as

$$P_S(S,L) = L^{\beta} \hat{p}(S/L^{\alpha}). \tag{30}$$

It is a multifractal fit that best describes the numerical data. In this section, we analyze how this multifractal dependence may appear. The lack of self-similarity is evidenced in Fig. 8, where we have plotted the $P_S(S,L)$ for the different sandpile lengths considered in this study. We have chosen the exponent a to get a good alignment of the tails of the PDFs [Fig. 8(a)]. Then, by looking at the PDF for small values of S/L^{α} [Fig. 8(b)] we see a systematic deviation from self-similarity. This is not surprising. From the analytical study that we presented in the preceding section, the L dependence in $P_S(S,L)$ is coming through the parameter p_1. As we obtained in Eq. (26), there is no self-similarity of $P_S(S,L)$. The only possible way of recovering the self-similar properties is by separating in $P_S(S,L)$ the contribution of the 1D and 2D avalanches. We can do so with the numerical results.

First, let us consider the PDF of the duration or size of the $n=1$ (1D) avalanches. We can see in Fig. 9 that this PDF is self-similar under a transformation of the type in Eq. (29) with $\alpha=\beta=0.5$. Since these PDFs have been normalized to 1, $\alpha=\beta$. For all the sizes of the sandpiles considered, all points of the PDF fall on top of the same curve.

For the 2D ($n \neq 1$) avalanches, the PDFs of the avalanche size are self-similar but with an exponent $\alpha=\beta=0.85$. This is shown in Fig. 10 for sandpile sizes varying from $L=200$ to 12 800. The scaling exponent is completely different from the scaling of the PDF of the avalanche size for the $n=1$ avalanches (Fig. 9). The analytical model gives a factor of 2 between these exponents. This is not the case of the numerical results. This discrepancy is not surprising because in the determination of these exponents in the self-similarity transformation, tails of the PDFs dominate and we know that the analytical model fails in giving those tails.

When we consider the 1D and 2D avalanches separately and for different values of the sandpile size, their PDFs seem to be self-similar. However, since we based the analysis on numerical results only, it is not possible to prove that the self-similarity is exact. However, if it is not exact, the symmetry breaking effects are small for the range of sandpile lengths considered here.

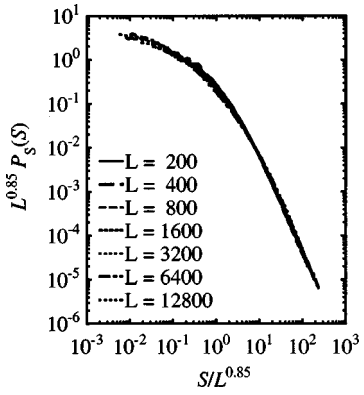

FIG. 10. PDF of the size of the 2D avalanches.

Another important issue to consider for the breakdown of the strict self-similarity of the avalanche PDFs is the role played by the avalanches that cross the edge of the sandpile. These avalanches are a small portion of the total number of avalanches, but they can modify the tail of the PDF because this class of avalanches includes the longest ones. The fraction of avalanches with flux out of the sandpile decreases as a fractional power of the size L. This dependence in L is shown in Fig. 11. These avalanches with flux out of the sandpile mostly start close to the edge. In Fig. 12 we have plotted the radial distribution of the starting points of the avalanches going through the edge boundary. Most of these avalanches start within 3% of the radius from the edge. These are mostly $n=1$ avalanches. Avalanches with $n\neq 1$ can start deep inside the sandpile, but the probability falls off exponentially from the edge. The width of the exponential can be considered as a measure of the edge region of the sandpile. From these data, we have determined that the normalized width scales as $W/L=0.64L^{-1/3}$. Therefore, as the size of the sandpile increases, this edge region becomes relatively less important and so has its effect on the overall contribution to the PDF.

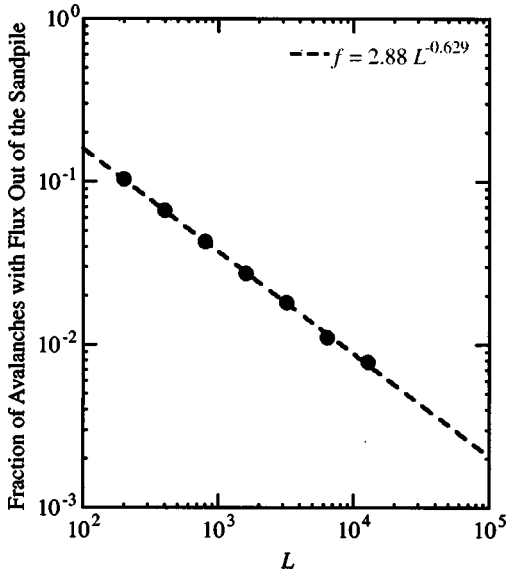

FIG. 11. Fraction of avalanches with flux out of the sandpile as a function of the sandpile length.

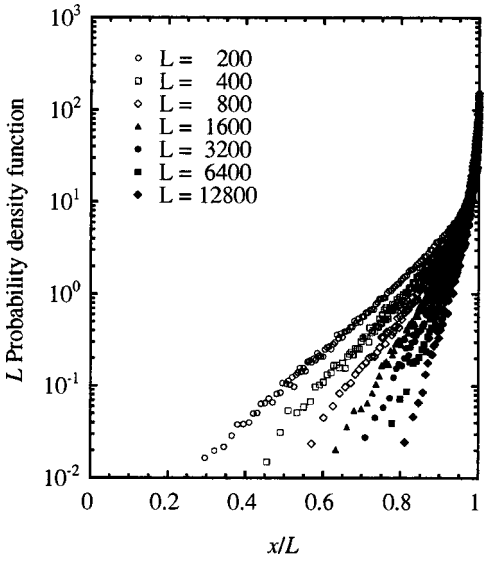

FIG. 12. Radial distribution of the starting points of the avalanches going through the edge boundary.

VII. CONCLUSIONS

In the sandpile model, the existence of two types of avalanches with different space-time structures causes a break of the self-similarity of the PDFs. The scaling of the avalanche size with L is different for the 1D and 2D avalanches. Therefore, when the scaling is studied with the combined effect of both types of avalanches, the effective scaling exponents vary with the parameter of the system. However, as L increases, the 2D avalanches tend to become dominant, and in the limit of infinite size, the scaling exponent should be given by the scaling of these avalanches.

The different dependence on L comes through the parameter p_1, the probability for a cell to be unstable when N_f grains of sand are added to this cell. This parameter carries the information on the correlation length of the sandpile slope, and through this the correlation length knows about the sandpile size.

There are also boundary effects. Those effects became smaller as the size of the sandpile increased, but the decrease of the effects goes as a fractional power of L, of about $-\frac{1}{3}$. Therefore, it is necessary to go to relatively large sandpile sizes to minimize those effects. In reality, they never disappear and they can become quite important when other dynamical effects, such as diffusion [9,10], are added to the sandpile dynamics.

ACKNOWLEDGMENTS

The authors gratefully acknowledge very stimulating and useful discussions with Barbara Drossel. This research is sponsored by Oak Ridge National Laboratory, managed by UT-Battelle, LLC, for the U.S. Department of Energy under Contract No. DE-AC05-00OR22725; the University of Alaska under Contract No. DE-FG03-99ER54551; and by the Dirección General de Investigación (Spain) under Project No. FTN2000-0924-C03-01.

[1] P. Bak, C. Tang, and K. Wiesenfeld, Phys. Rev. Lett. **59**, 381 (1987).
[2] P. H. Diamond and T. S. Hahm, Phys. Plasmas **2**, 3640 (1995).
[3] D. E. Newman *et al.*, Phys. Plasmas **3**, 1858 (1996).
[4] B. Drossel and F. Schwabl, Phys. Rev. Lett. **69**, 1629 (1992).
[5] L. P. Kadanoff *et al.*, Phys. Rev. A **39**, 6524 (1989).
[6] K. Schenk, B. Drossel, S. Clar, and F. Schwabl, Eur. Phys. J. B **15**, 177 (2000).
[7] K. Schenk, B. Drossel, and F. Schwabl (unpublished).
[8] T. Hwa and M. Kadar, Phys. Rev. A **45**, 7002 (1992).
[9] D. E. Newman, R. Sanchez, B. A. Carreras, and W. Ferenbaugh, Phys. Rev. Lett. **88**, 204304 (2002).
[10] R. Sanchez, D. Newman, and B. A. Carreras, Nucl. Fusion **41**, 247 (2001).
[11] M. N. Medvedev, P. H. Diamond, and B. A. Carreras, Phys. Plasmas **3**, 3745 (1996).